



# Novel gold dendritic nanoflowers deposited on titanium nitride for photoelectrochemical cells

Ming-Hua Shiao<sup>1</sup> · Chun-Ting Lin<sup>1</sup> · Hung Ji Huang<sup>1</sup> · Ping-Hsi Chen<sup>2</sup> · Bo-Huei Liao<sup>1</sup> · Fan-Gang Tseng<sup>3,4</sup> · Yung-Sheng Lin<sup>2</sup> 

Received: 14 February 2018 / Revised: 21 May 2018 / Accepted: 24 May 2018 / Published online: 14 June 2018  
© Springer-Verlag GmbH Germany, part of Springer Nature 2018

## Abstract

This study demonstrates the elaboration of a novel composite comprising gold dendritic nanoflowers (Au DNFs)/titanium nitride (TiN)/silicon (Si); this composite can be used for methanol oxidation reactions in alkaline electrolytes. Cyclic voltammograms showed that a thick (650 nm) Au DNFs/TiN/Si (L-DNFs-TiN) composite had double the oxidation current density of a thick (800 nm) Au DNFs/Si (L-DNFs-Si) composite in the presence of light illumination, whereas the oxidation current density for a thin (250 nm) Au DNFs/Si (S-DNFs-Si) composite and Au nanoparticles could not be determined. Chronoamperometry (CA) testing indicated that the L-DNFs-TiN could absorb light illumination more effectively than the L-DNFs-Si did. These results correspond to the broadband light absorption of TiN. Testing with continuous cyclic on/off light illumination showed a repeatable performance in CA, indicating that the proposed L-DNFs-TiN composite can be applied in photoelectrochemical cells in the future.

**Keywords** Gold · Titanium nitride · Methanol · Oxidation

✉ Yung-Sheng Lin  
linys@nuu.edu.tw

Ming-Hua Shiao  
mhshiao@narlabs.org.tw

Chun-Ting Lin  
chunting.pineapple.lin@gmail.com

Hung Ji Huang  
hjhuang@narlabs.org.tw

Ping-Hsi Chen  
as507132003@yahoo.com.tw

Bo-Huei Liao  
bohuei@narlabs.org.tw

Fan-Gang Tseng  
fangang@ess.nthu.edu.tw

<sup>1</sup> Instrument Technology Research Center, National Applied Research Laboratories, Hsinchu 300, Taiwan

<sup>2</sup> Department of Chemical Engineering, National United University, Miaoli 360, Taiwan

<sup>3</sup> Department of Engineering and System Science, Frontier Research Center on Fundamental and Applied Sciences of Matters, National Tsing Hua University, Hsinchu 300, Taiwan

<sup>4</sup> Research Center for Applied Sciences, Academia Sinica, Taipei 115, Taiwan

## Introduction

Photoelectrochemical cells (PECs) were first demonstrated in 1972 and have attracted considerable attention recently [1]. In direct methanol fuel cells, methanol can be photocatalytically oxidized by semiconductors under solar illumination; this reaction is especially well-known for TiO<sub>2</sub> semiconductors [1]. Metallic nanoparticles (NPs), such as Ag [2], Au [3], Pt [4], Pd [5], Ru [6], and Fe [7], can enhance the photocatalytic activity of TiO<sub>2</sub> by inhibiting electron–hole recombination and prolonging the photoexcitation of electrons. The decorated metallic NPs can also enhance absorption and utilize the visible light much efficiently. Although TiO<sub>2</sub> is chemically stable, environmentally friendly, abundant, and cheap, it can only be excited by ultraviolet light, which limits its applications in the visible light region [1]. Therefore, numerous other composited materials have been proposed to enhance photocatalytic activity.

Nanomaterials have large surface area-to-volume ratios and tend to enhance chemical reactivity. The wavelength or energy absorbed by nanosized metal materials is affected by the shapes and the sizes of nanostructures [8, 9]. Compared with one-dimensional nanomaterials, geometrically complex nanostructures have higher reactivity levels and specific reaction rates because they have larger specific surface areas and

lower densities. Porous morphology enhances mechanical robustness, maximizes harvesting of light, and promotes electrolyte diffusion [10]. It has been shown in a previous work that Au dendritic nanoflowers (Au DNFs) absorbed visible light more effectively than Au NPs [11].

Transition metal nitrides, specifically titanium nitride (TiN), have attracted considerable attention in connection with novel plasmonic materials [12, 13]. TiN exhibits optical properties analogous to noble metals and has become an alternative for practical plasmonic applications in the visible and infrared regions [14]. TiN is extremely hard and possesses remarkable electrical and thermal conductivity, chemical stability, and catalytic activity [15, 16]. Having an extremely high conductivity, namely  $4.5 \times 10^6$  S/m, nanostructured TiN performs well as an electrode material for applications in electrochemical energy storage [16]. Used as a catalyst, Pt-TiN demonstrated better performance in electrochemical oxidation of methanol than did Pt-TiO<sub>2</sub> [17].

The objective of this study was to investigate new materials for applications in PECs. Au DNFs with substantial specific surface areas and strong localized surface plasmon resonance (LSPR) for wide wavelengths [11] were combined with TiN with high electrical conductivity and broadband plasmonic properties in this study. A novel L-DNFs-TiN composite material was synthesized, and its performance in methanol oxidation reactions was tested.

## Materials and methods

### Sample preparation and characterization

Following a published method [18], the TiN thin film was deposited on silicon wafers by using a reactive high-power impulse magnetron sputtering system (HiPIMS, SPIK 2000A, Melec GmbH) in this study. In brief, the deposition chamber was pumped down to  $8 \times 10^{-6}$  Torr by a cryopump. The titanium sputtering target was a 4-in. disc. Ar-Ti HiPIMS discharge was operated at a pulsed on/off cycle of 45/955  $\mu$ s. An average power supply of 300 W was used in this sputtering process. The flow rates of argon and reactive nitrogen were fixed at 30 and 1.5 sccm, respectively.

A n-type silicon wafer (2 cm  $\times$  2 cm) was used as a substrate for the deposition of Au DNFs. Au DNFs were synthesized with a fluoride-assisted galvanic replacement reaction (FAGRR) [11]. In brief, a silicon wafer with and without TiN layer coating was dipped in a mixture of 10 mM chloroauric acid and buffered oxide etchant solution composed of 7% HF and 34% NH<sub>4</sub>F for 3 min. Table 1 shows the conditions of solutions and reaction times for Au NPs and Au DNFs.

The sample morphology and element analysis were conducted by scanning electron microscope (SEM; JSM-7800F, JEOL, Japan) and energy-dispersive X-ray spectroscopy (EDS), respectively. Crystalline properties were observed by X-ray diffraction (XRD; D2200, RIGAKU, Japan). The optical reflection was determined by ultraviolet-visible spectroscopy (U-3900/3900H, Hitachi, Japan).

### Electrochemical measurement

The electrochemical properties of the prepared Au samples were measured by a potentiostat (Jiehan 5600, Jiehan Technology, Taiwan) in a quartz three-electrode rectangular tank (10 cm  $\times$  10 cm  $\times$  10 cm) containing 500 mL of a mixture of 0.5 M NaOH and 1 M CH<sub>3</sub>OH. A tested sample with a defined 1-cm<sup>2</sup> projection area was utilized as the working electrode. A Pt-coated titanium mesh and a saturated calomel electrode were used as counter and reference electrodes, respectively. The scan range was from  $-0.2$  to  $0.6$  V [19], and a 30-mV/s scan rate was applied in cyclic voltammetry (CV). The effects of irradiation on the chronoamperometry (CA) of methanol oxidation were tested with a solar simulator (SADHUDESIGN; class B; 150 W;  $\lambda > 400$  nm).

## Results and discussion

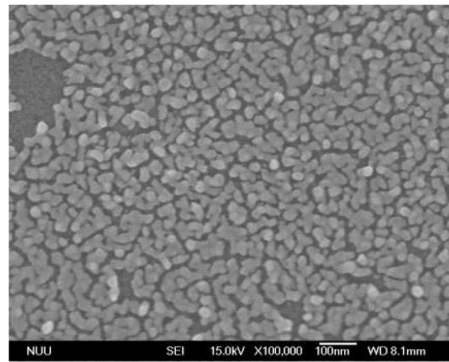
### Morphology and elements

Figure 1 presents SEM images of Au NPs, for thin (250 nm) and thick (800 nm) Au DNFs on silicon wafers. The Au NPs were isolated and distributed evenly (Fig. 1a) to form a uniform Au NP film (Fig. 1b) on the silicon surface. The S-DNFs-Si (Fig. 1c, d) exhibited a three-dimensional structure

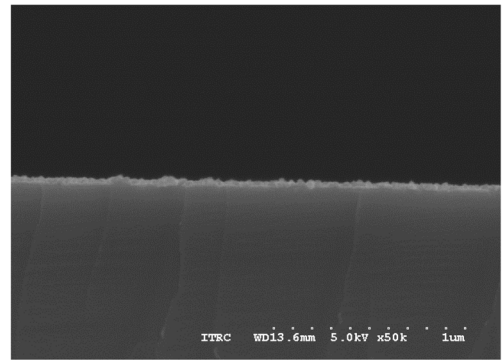
**Table 1** Condition of reactants and reaction time for different Au samples

Condition Group	Volume of 1 M HAuCl <sub>4</sub> (mL)	Volume of BOE (mL)	Volume of DI water (mL)	Reaction time (min)
Au NPs/Si	0.06	8	16	2.5
Thin (250 nm) Au DNFs/Si (S-DNFs-Si)	0.06	8	16	3
Thick (800 nm) Au DNFs/Si (L-DNFs-Si)	0.24	8	16	3
Thick (650 nm) Au DNFs/TiN/Si (L-DNFs-TiN)	0.24	8	16	3

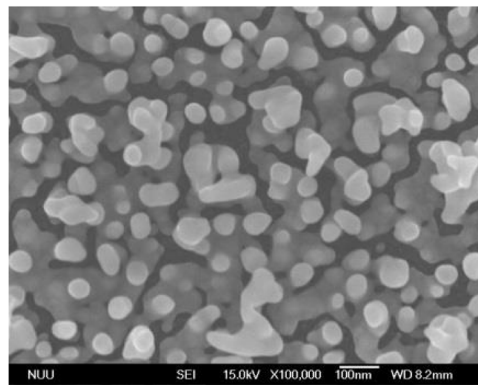
**Fig. 1** SEM examinations of Au. **a** Top view and **b** side view of Au NPs/Si; **c** top view and **d** side view of S-DNFs-Si; **e** top view and **f** side view of the L-DNFs-Si; **g** EDS spectrum of L-DNFs-Si



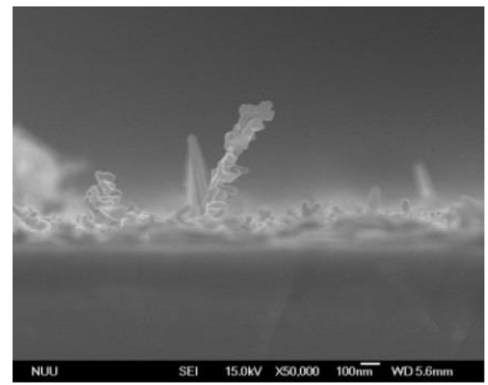
(a)



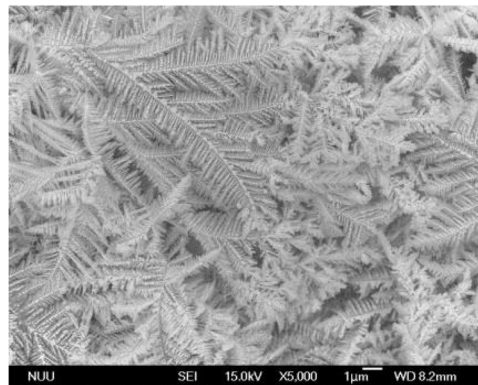
(b)



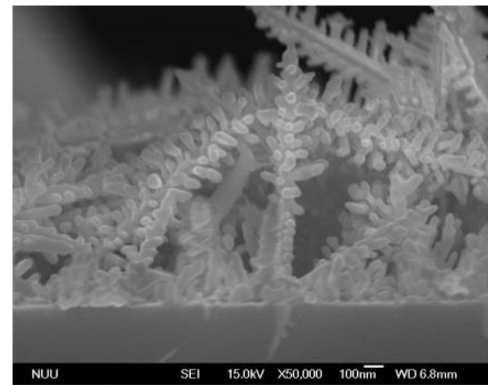
(c)



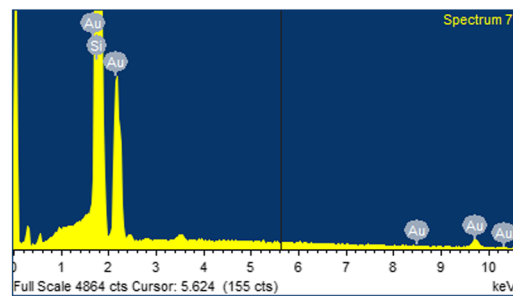
(d)



(e)

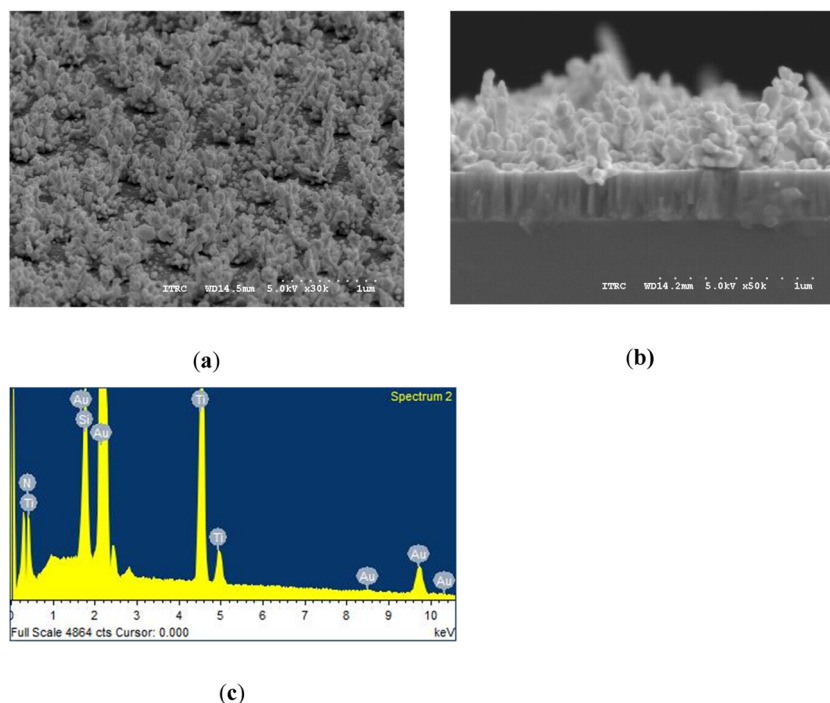


(f)



(g)

**Fig. 2** SEM examinations of L-DNFs-TiN. **a** Top view. **b** Side view. **c** EDS spectrum



and aggregation of Au NPs. This result was due to the prolonged synthesis reaction time for Au, which ranged from 2.5 to 3 min. The L-DNFs-Si (Fig. 1e, f) exhibited leaf shapes consisting of multiple levels of branches. The morphology of the sample L-DNFs-Si was growth with much more and longer Au DNFs than that of the sample S-DNFs-Si because a fourfold greater amount of  $\text{HAuCl}_4$  was applied in the Au synthesis of the L-DNFs-Si. The EDS spectrum revealed clear signals of Au and Si without any other by-products such as Cl or F, indicating that FAGRR deposited Au cleanly on the Si substrate [11].

Figure 2 presents SEM images and an EDS spectrum of the L-DNFs-TiN. The morphology of the L-DNFs-TiN was somewhat different from that of the L-DNFs-Si. Numerous dense NPs aggregated for the L-DNFs-TiN. The average deposited thicknesses of Au NPs/Si, the S-DNFs-Si, the L-DNFs-Si, and the L-DNFs-TiN were 50, 250, 800, and 650 nm, respectively. The deposited thickness of the L-DNFs-Si was greater than that of the L-DNFs-TiN because of the higher electron density generated in the FAGRR process to deposit Au. In the redox reactions of gold (III) chloride complex ions, for the same amount of fluoride, the Si reaction ( $\text{Si} + 6\text{F}^- \rightarrow \text{SiF}_6^{2-} + 4\text{e}^-$ ) [20] generated a fourfold greater number of electrons than the TiN reaction did ( $\text{TiN} + 3\text{HF}_2^- \rightarrow \text{TiF}_6^{2-} + \text{NH}_3 + \text{e}^-$ ) [21].

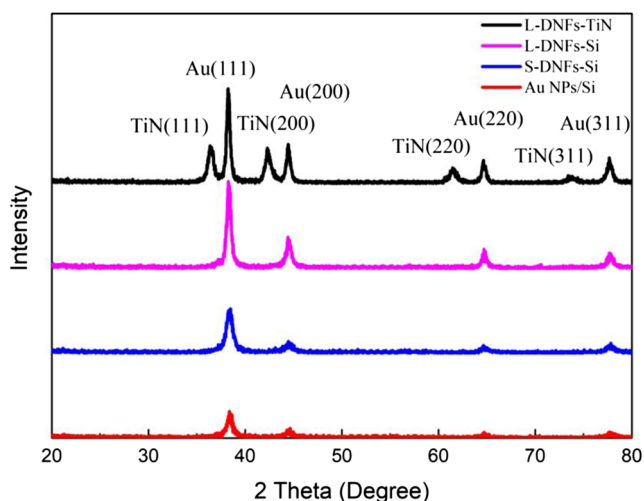


**Fig. 3** XRD patterns of Au NPs/Si, S-DNFs-Si, L-DNFs-Si, and L-DNFs-TiN

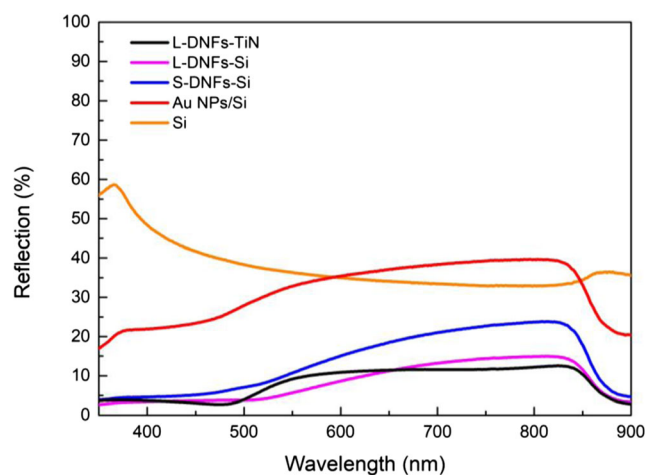
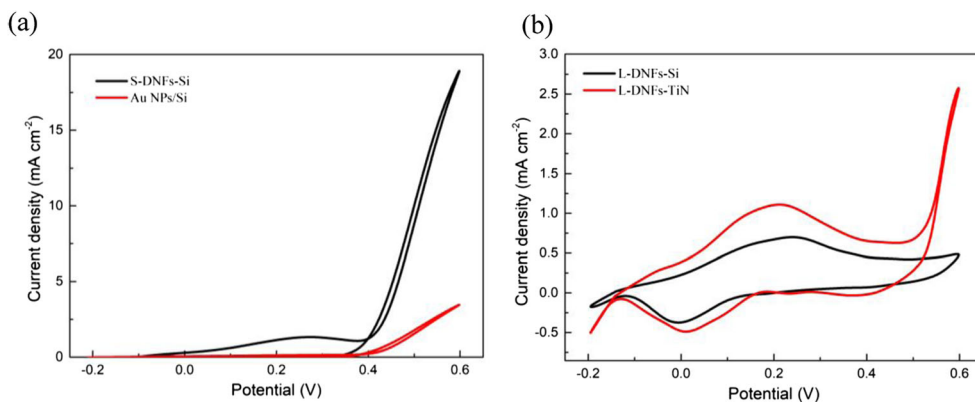


**Fig. 4** Reflection spectra of different samples

**Fig. 5** Cyclic voltammograms in 1 M CH<sub>3</sub>OH + 0.5 M NaOH for various working electrodes: **a** Au NPs/Si and S-DNFs-Si and **b** L-DNFs-Si and L-DNFs-TiN. A saturated calomel electrode served as the reference electrode



## Crystalline properties

Figure 3 shows the XRD patterns of Au DNFs and TiN. Four Au peaks, namely Au(111), Au(200), Au(220), and Au(311), were evident in all Au-containing samples. This result reflects the sharp cubic gold data and agrees with JCPDS 04-0784. Au(111) was the highest among the four Au peaks, indicating that the growth of Au has a strong preferential (111) orientation [22, 23]. The intensity of the Au peaks among different samples was in the following order: L-DNFs-Si, S-DNFs-Si, and Au NPs. In the L-DNFs-TiN sample, the growth of TiN(111), TiN(200), TiN(220), and TiN(311) was found. The growth of TiN was determined to have a preferential (111) orientation, which agrees with the TiN information in JCPDS38-1420.

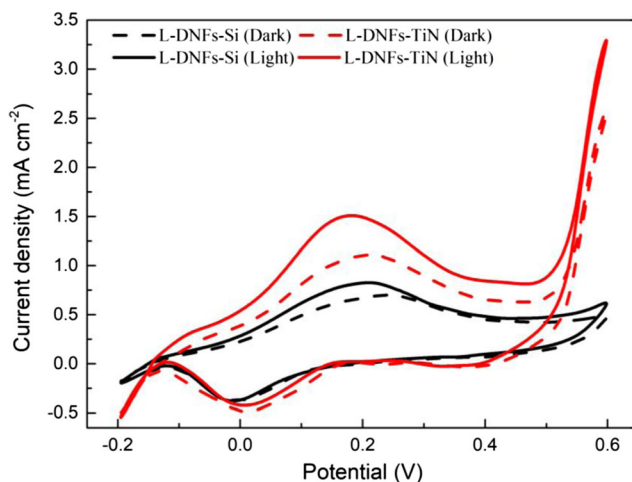
## Reflection

Figure 4 shows the optical reflection results of tested samples irradiated with light at 350–900 nm, close to the major spectral irradiance of sunlight. The polished Si wafer had a typical reflectance of approximately 40%, and the reflectance of Au NPs deposited on the Si wafer was greatly decreased in the 350–550 nm range. Compared with Au NPs, the geometric complexity of Au DNFs can engender multiple scattering of incident light and enhance light trapping [24]. Therefore, considerable antireflection behavior can be observed in Au DNFs, especially for thick samples. Relative to the reflectance result for the S-DNFs-Si, L-DNFs-Si exhibited superior antireflection properties in the wavelength range of 500–850 nm. The reflection characteristics of the L-DNFs-Si and L-DNFs-TiN were similar. However, the tested sample film thickness of the L-DNFs-TiN was lower than that of the L-DNFs-Si, indicating that TiN has enhanced resonant plasmon characteristics in the visible region [14, 25, 26]. A low reflection means a high absorption in this study. The layer having higher photocatalytic activities is the one having higher absorption. Thus, the improved photocatalytic activity may result from an improved light trapping mechanism.

Compared with the gold nanoparticles, the gold dendritic nanoflowers not only largely increase the deposited mass of gold on same substrate area, but also greatly increase the surface area as photocatalysts (Fig. 1). The largely increased surface area by the complex crystal structure not only brings in large amount of photocatalytic reaction simultaneously but also enhances the utilization efficiency through generation of localized surface plasmon resonance. The generation of localized surface plasmon resonance results in enhanced absorption of external illuminated light and wide-band decreased optical reflection.

## Electrochemical measurements

Figure 5 depicts the effects of different Au catalysts on the electrochemical properties of a methanol solution. The peak anodic (oxidation) current could not be determined for Au NPs/Si and S-DNFs-Si (Fig. 5a), but there was typical methanol polarization curves for L-DNFs-Si and L-DNFs-TiN (Fig. 5b). A comparison between CV plots for samples indicated that the thick Au DNFs on TiN/Si or Si were obviously



**Fig. 6** Cyclic voltammograms in 1 M CH<sub>3</sub>OH + 0.5 M NaOH for L-DNFs-Si and L-DNFs-TiN working electrodes with controlled light sources. A saturated calomel electrode served as the reference electrode

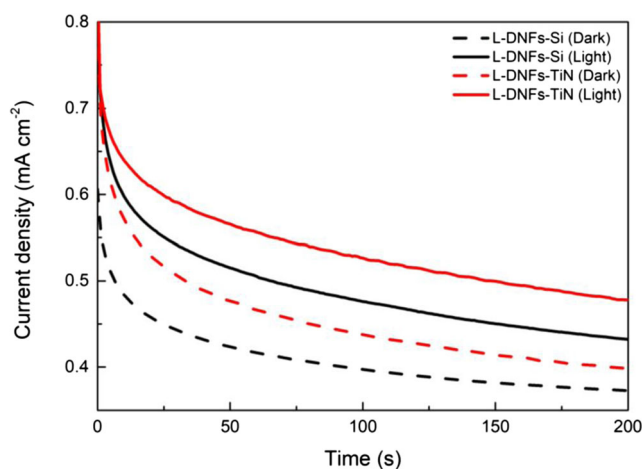


**Fig. 7** Chronoamperometric test of L-DNFs-Si and L-DNFs-TiN under different light conditions

active toward the methanol oxidation reaction process (Fig. 5b), but Au NPs/Si and the thin Au DNFs were not (Fig. 5a). Due to poor electron conductivity between the isolated Au NPs/Si and thin Au DNFs on the silicon wafer, Au NPs/Si and the S-DNFs-Si exhibited no signals of methanol oxidation [11].

Figure 6 illustrates the effects of light illumination on the electrochemical performance levels of the L-DNFs-Si and L-DNFs-TiN. As revealed by the photoresponse of the L-DNFs-Si, the oxidation peak current ( $I_p$ ) increased from 0.71 to 0.83 mA cm<sup>-2</sup>, whereas the peak voltage ( $V_p$ ) decreases from 0.25 to 0.22 V in the presence of light illumination. Regarding the L-DNFs-TiN,  $I_p$  increased from 1.12 to 1.52 mA cm<sup>-2</sup>, whereas  $V_p$  decreased from 0.22 to 0.19 V. These results provide direct evidence of photoenhanced methanol oxidation reactions with L-DNFs-Si and L-DNFs-TiN as photocatalysts. The L-DNFs-TiN had higher  $I_p$  and lower  $V_p$  values than the L-DNFs-Si did.

Figures 7 presents CA plots with 0.1 V polarization potential under dark and light conditions for the L-DNFs-Si and L-DNFs-TiN, respectively. Photocatalytic methanol oxidation

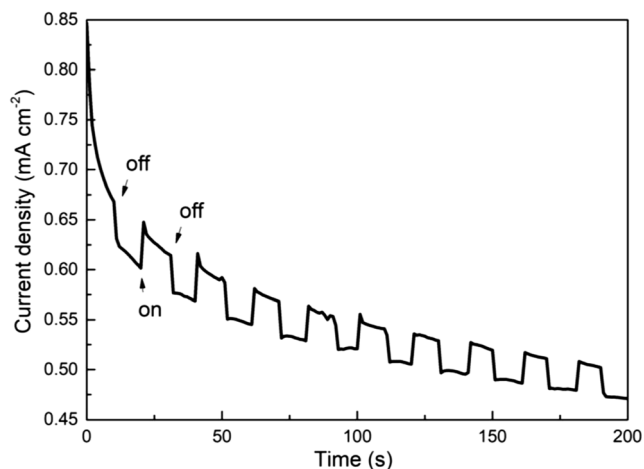
reactions can be also verified in this figure. Corresponding to the non-symmetrical result of the reduction-oxidation curve in Fig. 6, the increasing resistance of tested systems results in the decay of current density in CA plots. Regardless of light, L-DNFs-TiN has a higher current density than L-DNFs-Si. Compared with the dark condition, visible light was observed to have a current density enhancement in both the L-DNFs-Si and L-DNFs-TiN, agreeing with the current enhancement observed in Fig. 6. This demonstrates that the absorption of visible light enhances the photocatalytic methanol oxidation reactions, coinciding with the reflection data in Fig. 4. Table 2 further investigates current enhancement of L-DNFs-Si and L-DNFs-TiN under light treatment. Results indicate that there is a higher current enhancement in L-DNFs-TiN than L-DNFs-Si. The current enhancement of L-DNFs-Si decreases substantially with time, but little decrease for L-DNFs-TiN. The extra TiN layer reduced the absorption of light energy by Si substrate and has enhanced resonant plasmon characteristic for light. Furthermore, the ratio of current enhancement with light illumination by L-DNFs-TiN substrate retains longer time than that of Au DNFs/Si substrate. Therefore, an additional TiN layer provides superior utilization of incident light illumination compared to that of only L-DNFs-Si composite.

Figure 8 shows repeatability performance in continuous cyclic on/off light illumination testing over 200 s. The test conditions were the same as those presented in Fig. 7 for the L-DNFs-TiN. As revealed by the results, a steady performance of photocatalytic reaction could be observed after the second on/off test. The rising time and falling time of the response in current density are within 1 s. The generation of localized surface plasmon under light illumination is very fast; therefore, its effect turns on/off quickly. The almost instant response of current density with on/off light illumination switching indicates the practical utility of the L-DNFs-TiN composite in PECs.

In this study, 0.5 M NaOH was added to a methanol solution to enhance the oxidation reaction. A methanol oxidation reaction is more favorable with alkaline electrolytes than with neutral or acidic aqueous solutions. OH<sup>-</sup> ions scavenge holes

**Table 2** Comparison of current density and enhancement of L-DNFs-Si and L-DNFs-TiN under light treatment

Time (s)	Condition	L-DNFs-Si		L-DNFs-TiN	
		Current density $I$ ( $\mu\text{A cm}^{-2}$ )	Current enhancement $\Delta I$ ( $\mu\text{A cm}^{-2}$ )	Current density $I$ ( $\mu\text{A cm}^{-2}$ )	Current enhancement $\Delta I$ ( $\mu\text{A cm}^{-2}$ )
50	Dark	423.48	91.45	476.51	89.33
	Light	514.93	(21.6%)	565.84	(18.7%)
100	Dark	397.1	78.96	437.48	88.96
	Light	476.06	(19.9%)	526.44	(20.3%)
150	Dark	381.53	68.77	413.6	86.14
	Light	450.3	(18%)	499.74	(20.8%)
200	Dark	372.58	59.64	397.47	80.42
	Light	432.22	(16%)	477.89	(20.2%)



**Fig. 8** Chronoamperometric on/off light testing of L-DNFs-TiN

and thus reduce electron–hole recombination and accelerate the oxidation reaction. Alkaline electrolytes can improve the oxygen reduction reaction [27].

## Conclusions

This study proposes a novel L-DNFs-TiN composite for PECs. L-DNFs-TiN and L-DNFs-Si composites were determined to have oxidation current signals in methanol oxidation reactions with alkaline electrolytes. Regardless of light illumination, the L-DNFs-TiN exhibited better current density than the L-DNFs-Si. The system exhibited more current enhancement under light illumination than it exhibited under a dark condition, thus providing direct evidence of a photoenhanced methanol oxidation reaction. An additional absorbance of 400 nm in optical reflection appeared for TiN because of its unique semiconductor electron band transition mode. The cyclic on/off light illumination test presented a repeatability performance in CA, indicating that the synthesized L-DNFs-TiN composite has practical applications.

**Acknowledgments** The authors are grateful for the SEM analyses of Ms. Nancy Chu from the Instrument Technology Research Center, National Applied Research Laboratories.

**Funding information** The authors are grateful for the financial support of the Ministry of Science and Technology, Taiwan (contract numbers: MOST 105-2221-E-492-003-MY2 and MOST 106-2221-E-239-022).

## Compliance with ethical standards

**Conflict of interest** The authors declare that they have no conflict of interest.

## References

- Ahmad H, Kamarudin SK, Minggu LJ, Hasran UA, Masdar S, Wan Daud WR (2017) Enhancing methanol oxidation with a TiO<sub>2</sub>-modified semiconductor as a photo-catalyst. *Int J Hydrogen Energy* 42(14):8986–8996
- Krejčíková S, Matějová L, Kočí K, Obalová L, Matěj Z, Čapek L, Šolcová O (2012) Preparation and characterization of Ag-doped crystalline titania for photocatalysis applications. *Appl Catal B-Environ* 111-112:119–125
- Thomas J, Yoon M (2012) Facile synthesis of pure TiO<sub>2</sub>(B) nanofibers doped with gold nanoparticles and solar photocatalytic activities. *Appl Catal B-Environ* 111-112:502–508
- Sun B, Vorontsov AV, Smirniotis PG (2003) Role of platinum deposited on TiO<sub>2</sub> in phenol photocatalytic oxidation. *Langmuir* 19(8):3151–3156
- Fu P, Zhang P, Li J (2011) Photocatalytic degradation of low concentration formaldehyde and simultaneous elimination of ozone by-product using palladium modified TiO<sub>2</sub> films under UV254+185nm irradiation. *Appl Catal B-Environ* 105(1-2):220–228
- De Angelis F, Fantacci S, Selloni A, Nazeeruddin MK, Grätzel M (2007) Time-dependent density functional theory investigations on the excited states of Ru(II)-dye-sensitized TiO<sub>2</sub> nanoparticles: the role of sensitizer protonation. *J Am Chem Soc* 129(46):14156–14157
- Palanisamy B, Babu CM, Sundaravel B, Anandan S, Murugesan V (2013) Sol-gel synthesis of mesoporous mixed Fe<sub>2</sub>O<sub>3</sub>/TiO<sub>2</sub> photocatalyst: application for degradation of 4-chlorophenol. *J Hazard Mater* 252-253:233–242
- Lee S, Lee YW, Ahn H, Kim JH, Han SW (2017) Plasmon-enhanced electrocatalysis from synergistic hybrids of noble metal nanocrystals. *Curr Opin Electrochem* 4(1):11–17
- Bonyár A, Csarnovics I, Veres M, Himics L, Csik A, Kámán J, Balázs L, Kökényesi S (2018) Investigation of the performance of thermally generated gold nanoislands for LSPR and SERS applications. *Sens Actuat B-Chem* 255:433–439
- Kusior A, Wnuk A, Trenczek-Zajac A, Zakrzewska K, Radecka M (2015) TiO<sub>2</sub> nanostructures for photoelectrochemical cells (PECs). *Int J Hydrogen Energy* 40(14):4936–4944
- Lin CT, Chang MN, Huang HJ, Chen CH, Sun RJ, Liao BH, Chou Chau YF, Hsiao CN, Shiao MH, Tseng FG (2016) Rapid fabrication of three-dimensional gold dendritic nanoforests for visible light-enhanced methanol oxidation. *Electrochim Acta* 192:15–21
- Naldoni A, Shalaev VM, Brongersma ML (2017) Applying plasmonics to a sustainable future. *Science* 356(6341):908–909
- Naldoni A, Guler U, Wang Z, Marelli M, Malara F, Meng X, Besteiro LV, Govorov AO, Kildishev AV, Boltasseva A, Shalaev VM (2017) Broadband hot-electron collection for solar water splitting with plasmonic titanium nitride. *Adv Optical Mater* 5(15):1601031
- Venugopal N, Gerasimov VS, Ershov AE, Karpov SV, Polyutov SP (2017) Titanium nitride as light trapping plasmonic material in silicon solar cell. *Opt Mater* 72:397–402
- Lee CP, Lin LY, Vittal R, Ho KC (2011) Favorable effects of titanium nitride or its thermally treated version in a gel electrolyte for a quasi-solid-state dye-sensitized solar cell. *J Power Sources* 196(3):1665–1670
- Xie Y, Wang Y, Du H (2013) Electrochemical capacitance performance of titanium nitride nanoarray. *Mater Sci Eng B* 178(20):1443–1451

17. Musthafa OTM, Sampath S (2008) High performance platinized titanium nitride catalyst for methanol oxidation. *Chem Commun* 1: 67–69
18. Shiao MH, Lin CT, Zeng JJ, Lin YS (2018) Novel gold dendritic nanoforests combined with titanium nitride for visible-light-enhanced chemical degradation. *Nanomaterials* 8(5):282
19. Assiongbon KA, Roy D (2005) Electro-oxidation of methanol on gold in alkaline media: adsorption characteristics of reaction intermediates studied using time resolved electro-chemical impedance and surface plasmon resonance techniques. *Surf Sci* 594(1-3):99–119
20. Ye W, Shen C, Tian J, Wang C, Bao L, Gao H (2008) Self-assembled synthesis of SERS-active silver dendrites and photoluminescence properties of a thin porous silicon layer. *Electrochem Commun* 10(4):625–629
21. Carraro C, Maboudian R, Magagnin L (2007) Metallization and nanostructuring of semiconductor surfaces by galvanic displacement processes. *Surf Sci Rep* 62(12):499–525
22. Lahiri A, Wen R, Kuimalee S, Kobayashi S, Park H (2012) One-step growth of needle and dendritic gold nanostructures on silicon for surface enhanced Raman scattering. *CrystEngComm* 14(4): 1241–1246
23. Lahiri A, Wen R, Kuimalee S, Chowdhury A, Kobayashi S, Zhang L, Wang P, Fang Y (2013) Photo-assisted control of gold and silver nanostructures on silicon and its SERRS effect. *J Phys D-Appl Phys* 46(27):275303
24. Jung JY, Guo Z, Jee SW, Um HD, Park KT, Lee JH (2010) A strong antireflective solar cell prepared by tapering silicon nanowires. *Opt Mater Express* 18(S3):A286–A292
25. White N, Campbell AL, Grant JT, Pachter R, Eyink K, Jakubiak R, Martinez G, Ramana CV (2014) Surface/interface analysis and optical properties of RF sputter-deposited nanocrystalline titanium nitride thin films. *Appl Surf Sci* 292:74–85
26. Zhao J, Lin J, Wei H, Li X, Zhang W, Zhao G, Bu J, Chen Y (2015) Surface enhanced Raman scattering substrates based on titanium nitride nanorods. *Opt Mater* 47:219–224
27. Liao Q, Li L, Chen R, Zhu X, Wang H, Ye D, Cheng X, Zhang M, Zhou Y (2015) Respective electrode potential characteristics of photocatalytic fuel cell with visible-light responsive photoanode and air-breathing cathode. *Int J Hydrogen Energ* 40(46):16547–16555